Bioorganic Chemistry 91 (2019) 103094

Contents lists available at ScienceDirect

Bioorganic Chemistry

journal homepage: www.elsevier.com/locate/bioorg

Design, synthesis and biological evaluation of 4-aminoquinoline-guanylthiourea derivatives as antimalarial agents

Shweta Bhagat[a], Minhajul Arfeen[a], Gourav Das[a], Mridula Ramkumar[b], Shabana I. Khan[c], Babu L. Tekwani[c], Prasad V. Bharatam[a,*]

[a] Department of Medicinal Chemistry, National Institute of Pharmaceutical Education and Research, Sector-67, S.A.S. Nagar 160062, Punjab, India
[b] Department of Pharmacoinformatics, National Institute of Pharmaceutical Education and Research, Sector-67, S.A.S. Nagar 160062, Punjab, India
[c] National Center for Natural Products Research, University of Mississippi, MS 38677, USA

ARTICLE INFO

Keywords:
4-Aminoquinoline
Guanylthiourea
*Pf*DHFR
Molecular docking
Molecular dynamics
In vitro studies

ABSTRACT

Guanylthiourea (GTU) has been identified as an important antifolate antimalarial pharmacophore unit, whereas, 4-amino quinolones are already known for antimalarial activity. In the present work molecules carrying 4-aminoquinoline and GTU moiety have been designed using molecular docking analysis with *Pf*DHFR enzyme and heme unit. The docking results indicated that the necessary interactions (Asp54 and Ile14) and docking score (−9.63 to −7.36 kcal/mmol) were comparable to WR99210 (−9.89 kcal/mol). From these results nine molecules were selected for synthesis. *In vitro* analysis of these synthesized compounds reveal that out of the nine molecules, eight show antimalarial activity in the range of 0.61–7.55 μM for *Pf*D6 strain and 0.43–8.04 μM for *Pf*W2 strain. Further, molecular dynamics simulations were performed on the most active molecule to establish comparative binding interactions of these compounds and reference ligand with *Plasmodium falciparum* dihydrofolate reductase (*Pf*DHFR).

1. Introduction

Malaria has been regarded as greatest health tragedies of 21st century. According to the world malaria report 2018 published by world health organization, approximately 219 million new cases were reported in 2017. The numbers showed an increase of 2 million cases from the previous year [1]. The number of global deaths reported in the year 2017 was 435,000 out of which 61% of total malaria deaths is accounted for children aged under 5 years [1]. In the absence of effective vaccines, chemotherapy remains the first line of defense against malaria [2]. However, this first line of defense received setback when reports of chloroquine resistant plasmodium strains surfaced [3]. Subsequently, the artemisinin and its derivative became an important component in the malarial therapy [4]. This class of drugs were considered as the only drugs with the potential to treat multi drug resistant strains of malaria. Given the recent reports of resistance that emerged from Southeast Asia, on 21st century antimalarial "stars" artemisinin and its derivative, the current state of antimalarial therapy is extremely worrisome [5], thus there is challenge and urgent need to develop cost effective antimalarial agents.

Regardless of the reports of resistance to quinoline based drugs, which act on heme, they are still being exploited as lead compounds for the design of new antimalarials [6], because, the resistance against this class of drugs is more of a compound specific than target oriented [7]. Earlier it was established that GTU derivatives exhibit anti-malarial activity [8]. Therefore, in this work 4-aminoquinoline (QN) moiety was conjugated with previously identified guanylthiourea (GTU) moiety (identified as antifolate) to design new antimalarial compounds (Fig. 1). The two chemical entities were connected with linker chain in order to identify the suitable linker for antimalarial action. Molecular docking analysis was done to screen the designed molecules. Nine most promising molecules were taken up for synthesis. Cell based *in vitro* studies [5c,9] were carried out to estimate the antimalarial potential of the synthesized molecules. Further, cytotoxic studies were carried out to establish the safety of these molecules to humans.

2. Rational design

The already known *Pf*DHFR inhibitors (pyrimethamine and cycloguanil) and lead compound (WR99210) have 2,4-diaminopyridine and 2,4-diamino-1,3,5-triazine moieties, respectively [10]. GTU is nitrogen rich species and provides sufficient number of H-bond acceptor and donor group similar to that of pyridine and triazine moiety [11]. The GTU moiety is particularly flexible because of the open chain character,

* Corresponding author.
E-mail address: pvbharatam@niper.ac.in (P.V. Bharatam).

https://doi.org/10.1016/j.bioorg.2019.103094
Received 31 January 2019; Received in revised form 10 May 2019; Accepted 26 June 2019
Available online 02 July 2019

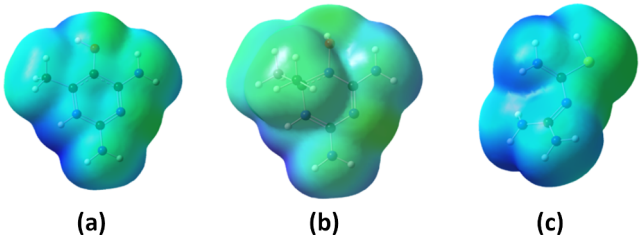

Fig. 1. MESP surfaces of protonated pyrimidine (a), triazine (b) and GTU (c). Blue color represents positive potential and red color represents negative potential. Due to the overall protonated state of the molecules, there is no negative potential observed. All the structures were optimized using B3LYP method in Gaussian 09 and MESP plots were generated using Gauss View.[13]

but is also sufficiently rigid due to the presence of conjugated double bonds, which allow it to acquire a close interaction with the Asp54 of *Pf*DHFR in the molecular recognition site [10d,12]. To support the replacement of triazine and pyrimidine moieties with GTU, molecular electrostatic surface potential (MESP) analysis was performed. The MESP surfaces of the three moieties in the protonated form are shown in Fig. 1. This surface property establishes that the required electronic characteristics present on the surface of GTU are similar to that of the 2,4-diamino-1,3,5-triazine and 2,4-diaminopyridine moieties. Hence, replacing pyridine and triazine moieties with GTU was found worthwhile for further widening this database.

Fig. 2 shows a schematic diagram of two pharmacophoric units QN and GTU connected together using a flexible linker. The flexible linker was varied to have 4, 5, and 6 carbon atom chain so that the two pharmacophore may show antimalarial action against both *Pf*DHFR and heme. Several modifications in literature reported the addition of 4–12 atom linkers in the QN-antifolate molecules (Fig. 3).

A virtual library of 100 molecules with combinations of QN, varying length linker chains and the GTU moiety were prepared. These species were subjected to molecular docking analysis. Molecular docking studies were performed using Glide module of Schrödinger on *Pf*DHFR (PDB ID: 1J3I-wild type and PDB ID: 1J3K-mutant) and Heme (extracted from PDB ID: 2HBS; Fig. S1 of supporting information) crystal structures for analysis [15]. Pharmacoinformatic tools were used for predicting the drug like characters of the prepared library of compounds. From combined results of these two studies, nine molecules were selected for synthesis. GTU derivatives designed with 7-chloroquinoline (**4a-c**), 7-trifluoromethylquinoline (**4d-f**) and 2,8-bis(trifluoromethyl)quinoline (**4g-i**) moieties (Scheme 1) showed the highest docking scores and most of the favorable interactions when compared to WR99210 (with *Pf*DHFR) and chloroquine (with heme). Molecular docking studies confirmed that hydrocarbon linker with two to four carbon atoms are most suitable to provide the favorable interactions (Table 1). Whereas, the compounds with linker more than six carbon atoms fail to accommodate in the active site of *Pf*DHFR enzyme and thus lack interactions for molecular recognition. It was observed that the bound ligand (WR99210) binds deep in the cavity (in both wild (1J3I) and quadruple mutant (1J3K) *Pf*DHFR) forming bidentate H-bonding with Asp54 and H-bonding with Cys15, Ile14, $Ile_{1J3I}164$/$Leu_{1J3K}164$. It shows π-π stacking interaction with Phe58. In case of 1J3K (quadruple mutant *Pf*DHFR), WR99210 forms salt bridge with Asp54. The interactions shown by pyrimethamine are very similar to WR99210, however, it lacks the hydrophobic interactions with Phe116, Pro113, Leu119, Val45 and Met45. Also, in case of quadruple mutant, it was observed that the conformations of pyrimethamine were not stable due to Asn108 mutation.

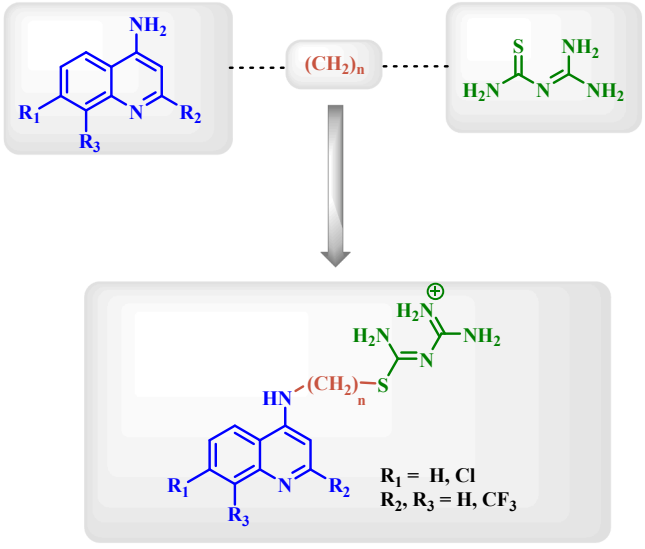

Fig. 2. Schematic representation of the fusion of different moieties to design the hybrid molecule.

Druglikness studies showed that for all the selected molecules, the molecular weight is less than 500 gm/mol. Their logP value is less than 5, hydrogen bond donors are less than 5, and hydrogen bond acceptors are less than 10. The total polar surfaces for all molecules under consideration are within the range of 90–140 $Å^2$ [16]. The detailed results are listed in Table T1 of the supporting information.

3. Synthesis

Scheme 1 shows the complete synthetic scheme for the synthesis of compounds **4a-i**. 4,7-dichloroquinoline, 4-chloro-7-trifluoromethyl quinoline and 2,8-bis(trifluoromethyl)-4-quinolinol were taken as the starting material for **4a-c**, **4d-f**, and **4g-i**, respectively. For the synthesis of **1g-i**, 4-quinolinol was converted to 4-chloroquinoline using phosphoryl oxychloride as chlorinating agent [17]. The alkyl chains containing 2/3/4 carbon atoms were attached to the 4-chloroquinoline (**2a-i**) intermediate by reacting aminoalcohols (ethanolamine/propanolamine/butanolamine) under neat conditions to form intermediates **2a-i** [18]. The quinoline aminoalcohol was converted to bromide derivative (**3a-i**) using HBr-H_2SO_4 as brominating agent [19]. The final step was the *S*-alkylation of guanylthiourea with quinoline aminoalkylbromide (**3a-i**) under reflux conditions in acetonitrile to give the final product as bromide salt, **4a-i** [8a,8c,20].

4. Biological evaluation

Cell based *in vitro* analysis was carried out for the synthesized molecules on chloroquine-pyrimethamine sensitive strain (*Pf* D6) and chloroquine-pyrimethamine resistant strain (*Pf* W2). Cytotoxicity studies for the compounds were performed on vero cell lines. Table 2 shows activity in μM range and relative inhibition (RI) (antimalarial activity against CQ-S D6 strain vs CQ-R W2 strain) values. Compound **4c** showed the highest activity against both *Pf* D6 strain (0.61 μM) and *Pf* W2 strain (0.43 μM) followed by **4b** and **4a**. The RI value is more (1.42) for **4c** as compared to other compounds which indicates that it inhibits chloroquine-resistant *Pf* W2 strain more effectively than chloroquine-sensitive *Pf* D6 strain.

The 4-aminoquinoline based derivatives (**4a-c**) showed relatively better activity compared to 7-trifluoromethyl quinoline (**4d-f**) and mefloquine based derivatives (**4g-i**). Also, compounds with four atoms linker exhibited better activity for 4-aminoquinoline based derivatives. The analogs with two atoms linker were more active for trifluoromethyl quinoline derivatives and the analogs with three atoms linker were more active for mefloquine based derivatives. The better activity of **4a-c** can be due to the chlorine substituent in the quinolone moiety which is a smaller group and may provide halogen bonding in the solvent accessible region of the enzyme. However, the trifluoromethyl group in **4d-f** is a bulky group and may result in unfavourable interactions or

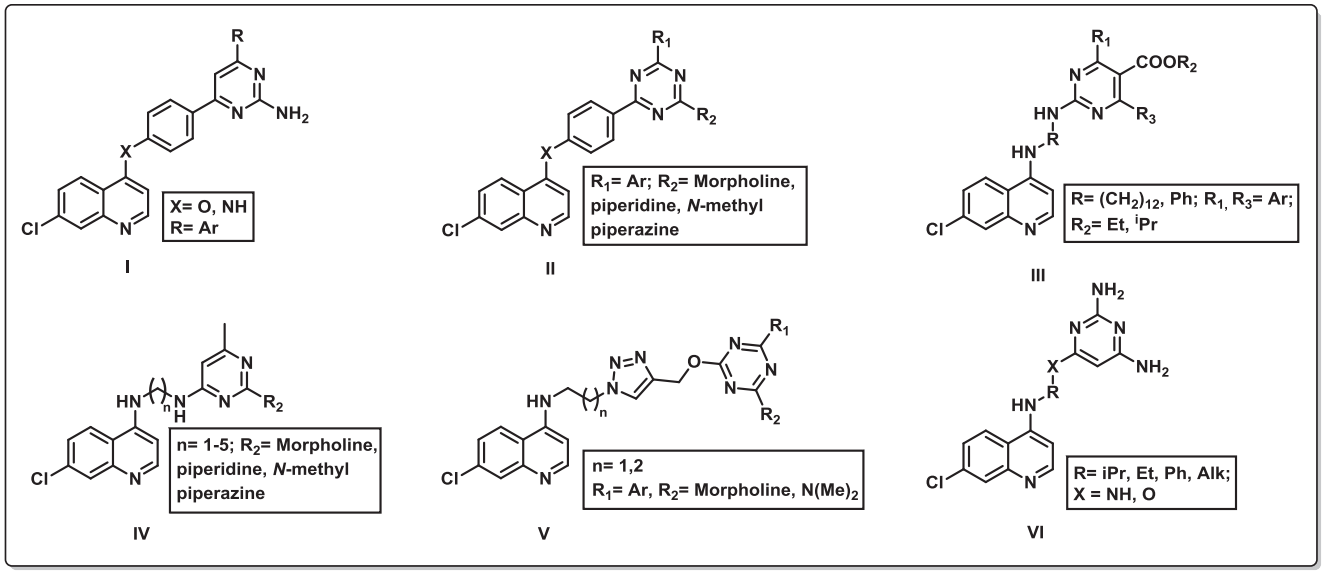

Fig. 3. Examples of quinoline-antifolate based antimalarial molecules.[14].

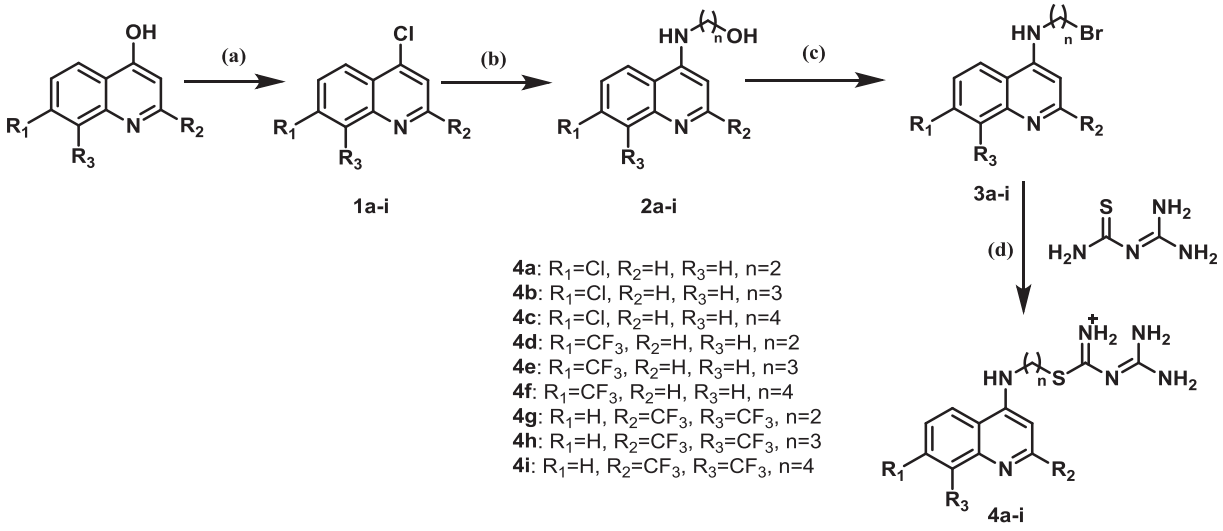

Scheme 1. (a) $POCl_3$, 150 °C, 3 h; (b) amino alcohol, 130 °C, 3 h; (c) HBr, a few drops of H_2SO_4, 140 °C, 6 h; (d) guanylthiourea, CH_3CN, reflux, 12–24 h.

Table 1
Molecular docking studies of selected nine molecules on *Pf*DHFR (PDB ID: 1J3K and 1J3I, and Heme (extracted from PDB ID: 2HBS).

S. No.	R_1	R_2	R_3	n	*Pf*DHFR (1J3I)		*Pf*DHFR (1J3K)		Heme
					G_{score}	Interactions[c]	G_{score}	Interactions[c]	
WR99210	–	–	–	–	−9.89	I14, C15, D54, I164	−9.64	I14, C15, D54[d], L164	–
CLQ[a]	–	–	–	–	–	–	–	–	−4.01
Pyr[b]	–	–	–	–	−8.32	I14, C15, D54[d], I164, F58	−7.81	I14, C15, D54[d], F58, L164, Y183	–
4a	Cl	H	H	2	−7.36	D54	−7.73	D54[d], F58	−5.56
4b	Cl	H	H	3	−7.84	D54, A16	−9.31	D54	−5.34
4c	Cl	H	H	4	−8.31	I14, D54[d], A16	−7.52	D54[d]	−5.54
4d	CF_3	H	H	2	−8.00	I14, D54, I164	−7.57	D54, L164, F58	−4.93
4e	CF_3	H	H	3	−8.06	D54, I164, F116	−6.82	D54, F58	−5.00
4f	CF_3	H	H	4	−9.01	I14, D54	−7.74	A16, D54[d]	−5.26
4g	H	CF_3	CF_3	2	−8.73	I14, D54, I164	−7.12	I14, C15, D54, L164, F58, N108	−4.58
4h	H	CF_3	CF_3	3	−9.15	D54	−8.43	A16, D54[d]	−4.99
4i	H	CF_3	CF_3	4	−9.63	D54	−8.28	D54, S111	−5.05

[a] Chloroquine (CLQ).
[b] Pyrimethamine (Pyr).
[c] Amino acids are given in one letter code.
[d] Salt bridge.

Table 2
In vitro results of the synthesized compounds in *Pf* D6 strain, *Pf* W2 strain and vero cell lines with IC_{50}, standard inhibition (SI) and relative inhibition (RI) values.

Compd. No.	*Pf* D6 strain	*Pf* W2 strain	RI[#]	Cytotoxicity (vero cell lines) IC_{50} (μM)
	IC_{50} (μM)	IC_{50} (μM)		
4a	2.25	3.71	0.61	> 11.79
4b	1.56	2.13	0.73	> 11.39
4c	0.61	0.43	1.42	> 11.02
4d	1.86	2.95	0.63	> 10.89
4e	2.85	3.21	0.89	> 10.55
4f	2.80	6.06	0.46	> 10.23
4g	7.55	8.04	0.94	> 9.42
4h	5.54	7.21	0.77	> 9.17
4i	> 8.93	> 8.93	1.00	> 8.93
Chloroquine	0.04	0.39	0.10	NC
Pyrimethamine	0.01	NA	–	18.2

[#] RI = IC_{50} (*Pf*D6)/IC_{50} (*Pf* W2).

steric clashes. This is further supported by the fact that **4g-i** are the least active compounds in the given group and contain two trifluoromethyl groups.

5. Molecular dynamics

Molecular dynamics simulations were carried out for 1J3I-WR, 1J3K-WR, 1J3I-4c and 1J3K-4c complexes to evaluate the atomic level interactions of the hybrid molecule (**4c**) with the wild type and quadruple mutant *Pf*DHFR enzyme and also to compare these interactions with the standard WR99210 (WR) molecule. The stability of the complexes was determined by calculating the RMSD values from the initial coordinates for each of the complexes (see supporting information, Fig. S2). The systems attained equilibrium after 4 ns of the production run. All the four complexes were stable throughout the whole simulation run of 20 ns. Molecular Mechanics Poisson-Boltzmann Surface Area (MM-PBSA) energy decomposition analysis was performed using AMBER 11.0 program (last 4 ns). The results of binding energy obtained from MM-PBSA for **4c** with *Pf*DHFR were on par with that of the co-crystallized ligand, as shown in Fig. 4. The energy difference of ~7 kcal/mol in case of the wild type *Pf*DHFR may be attributed to the stronger van der Waals interactions in case of WR due to aromatic triazine moiety and high polar solvation energy for **4c**. It was also observed that the binding of **4c** molecule was not affected by mutations present in the *Pf*DHFR as the binding affinities for both WR and **4c** in the quadruple mutant (1J3K) were comparable. Residue wise decomposition analysis suggests that **4c** has the highest binding affinity for Asp54 and Ile14,

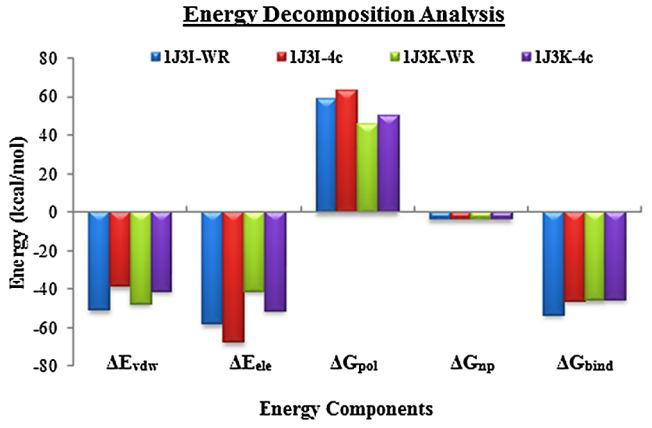

Fig. 4. Bar graph depicting the binding energy and its components for WRA and **4c** complexed with wild (1J3I) and quadruple mutant (1J3K) type *Pf*DHFR.

which are the major amino acids for molecular recognition in both 1J3I and 1J3K (Fig. S3). The hydrogen bond occupancy was also analysed which indicated that WR forms a bifurcated H-bond with Asp54 as the occupancy is more than 100% (Fig. S4). The detailed binding poses are given in the supporting information (Figs. S5–S8).

6. Conclusions

Structure based drug design approach was used to design a library QN-GTU hybrid molecules with different quinoline substitutions and variable hydrocarbon chain as linker. Molecular docking analysis was carried out on the wild type *Pf*DHFR (PDB ID: 1J3I), mutant type *Pf*DHFR (PDB ID: 1J3K) and heme (isolated from PDB ID: 2HBS) and results were compared with WR99210 (co-crystallized ligand) and chloroquine. Property filters were applied to determine the drug likeness of these molecules. Nine molecules were finally selected for synthesis from molecular docking and property filter analysis. The selected compounds **4a-i** were then synthesized by attachment of the linker on the quinoline moiety. The GTU moiety was linked through *S*-alkylation with the final yield of the compounds in the range of 35–65%. Biological testing was done on chloroquine-pyrimethamine sensitive (D6 strain) and resistant (W2 strain) *P. falciparum*. Eight compounds showed antimalarial activity with IC_{50} values in the range of 0.43–8.04 μM. None of these compounds showed cytotoxicity against vero cells, which indicates that all the compounds were non-cytotoxic at the highest concentrations tested. Compounds **4a-c,** with 4-aminoquinoline moiety showed the better activity compared to the corresponding 7-trifloromethyl quinoline (**4d-f**) and mefloquine derivatives (**4g-i**). Six atom linker 4-aminoquinoline derivative, **4c**, showed highest activity i.e. 0.6 μM against *Pf* D6 strain and 0.4 μM against *Pf* W2 strain. In case of 7-trifloromethyl quinoline derived compounds (**4d-f**), the IC_{50} values were in the range of 2.85–1.86 μM for *Pf* D6 strain and 2.95–6.06 μM for *Pf* W2 strain. The compound with 4 atom linker chain (**4d**) was found to be most active. The mefloquine based derivatives (**4g-i**) were less active with IC_{50} values in the range of 5.54– > 8.9 μM and 7.2– > 8.9 μM against *Pf* D6 strain and *Pf* W2 strain respectively.

To determine the binding interaction details of **4c** on *Pf*DHFR enzyme (both wild, 1J3I, and mutant type, 1J3K), molecular dynamics (MD) simulations studies were carried out. In 1J3I, co-crystallized ligand (WR99210) displayed 7 kcal/mol higher binding energy (53.5 kcal/mol) as compared to **4c** (46.2 kcal/mol) which showed that **4c** has comparable binding energy (MM-PBSA) of −45 kcal/mol to 1J3K when compared with the co-crystallized ligand where binding energy is −46 kcal/mol. The residue wise decomposition energy analysis shows that **4c** exhibits similar interactions as shown by WR99210. Binding energy of **4c** with Ile14 is comparable to that of WR99210 but that with Asp54, it is 3 kcal/mol less than WR99210. However, **4c** forms a bidentate H-bond with Asp54 energy with an occupancy of > 100% (~50% for WR99210).

7. Experimental section

Proton NMR experiments and carbon-13 NMR experiments were recorded on Bruker Advance DX 400 MHz spectrometer. Chemical shifts were reported in parts per million relative to tetramethylsilane as internal standard. Splitting pattern were designated as s, singlet; d, doublet; dd, doublet of doublet; m, multiplet. Thin layer chromatography (TLC) analyses were performed on precoated silica gel plates (GF 254, Merk). Mass spectrometry was performed using Shimadzu QP5000 mass spectrometer and LTQ Finnigen MAT. IR spectroscopy was performed using Perkin Elmer FTIR with ATR and IR microscope Synthesis Monitoring System. HRMS was performed using instrument XEVO G2-XS QTOF.

7.1. Typical procedure for the synthesis of S-alkylated quinoline derivatives

7.1.1. Synthesis of 4-chloro-2,8-bis(trifluoromethyl)quinoline [21] (1g)

Phosphorous oxychloride (1.02 g, 3.56 mmol) under nitrogen atmosphere was added to a 50 mL round bottom flask fitted with a condenser and stirred at 70 °C until all the solid was dissolved (usually within 5–10 min). 4-quinolinol (1 g, 3.56 mmol) portion wise was added to this hot solution and the bath temperature was increased to 150 °C. Stirring was continued at this temperature for 2 h. After allowing to cool to room temperature, the reaction mixture was quenched by the addition of ice-cold water (10 mL) and stirring was continued for another 1 h. The precipitated chloride was then filtered through a sintered funnel by washing with an excess of purified water and dried under vacuum to obtain a colourless solid **1g,** as a single spot on TLC (1.16 g). The chloride was then carried to the next step without further purification [17].

7.1.2. Synthesis of 2-((7-chloroquinolin-4-yl)amino)ethan-1-ol [22] (2a)

4,7-Dichloroquinoline (2 g, 10 mmol) was heated with stirring in neat aminoethanol (10 mL) at 130 °C for 5 h. The mixture was then allowed to cool at room temperature and poured into cold water during which the compound precipitated. The precipitate was filtered using a Buchner funnel dried under vacuum to get 2-((7-chloroquinolin-4-yl) amino)ethan-1-ol (**2a)** as a white solid in 95% yield. ^{1}H NMR (400 MHz, CD_3SOCD_3) δ = 8.36 (d, J = 5.8, 1H), 8.09 (d, J = 9.0 Hz, 1H), 7.78 (d, J = 2.0 Hz, 1H), 7.40 (dd, J = 2.0 Hz, J = 9.0 Hz, 1H), 6.57 (d, J = 5.5 Hz, 1H), 3.86 (t, J = 5.8, 2H), 3.51 (t, J = 5.8, 2H); ^{13}C NMR (100 MHz, CD_3SOCD_3): δ = 151.43, 151.03, 148.28, 134.92, 126.21, 124.62, 122.83, 118.30, 98.33, 59.33, 44.81; MS (LTQ): m/z calculated for $C_{11}H_{11}ClN_2O^+$ $[M+H]^+$ 223.06; found 223.03.

The remaining quinoline aminoalcohol derivatives (**2b-i**) were prepared following this typical procedure [18]. Intermediates **2d-i** were determined by change in the TLC pattern and LTQ, thus were directly taken to the next step for synthesis of bromide derivatives.

7.1.3. 3-((7-chloroquinolin-4-yl)amino)propan-1-ol (2b)

White solid in 90% yield. ^{1}H NMR (400 MHz, CD_3SOCD_3) δ = 8.36 (d, J = 5.5, 1H), 8.07 (d, J = 9.0 Hz, 1H), 7.78 (d, J = 2.2 Hz, 1H), 7.41 (dd, J = 2.0 Hz, J = 9.0 Hz, 1H), 6.56 (d, J = 5.5 Hz, 1H), 3.37 (t, J = 6.0, 2H), 3.49 (t, J = 7.0, 2H), 1.98 (m, 2H); ^{13}C NMR (100 MHz, CD_3SOCD_3): δ = 151.42, 150.91, 148.09, 134.94, 126.08, 124.59, 122.81, 117.32, 98.18, 59.37, 39.83, 30.71; MS (LTQ): m/z calculated for $C_{12}H_{14}ClN_2O^+$ $[M+H]^+$ 237.08; found 236.99.

7.1.4. 4-((7-chloroquinolin-4-yl)amino)butan-1-ol (2c)

White solid in 92% yield. ^{1}H NMR (400 MHz, CD_3SOCD_3) δ = 8.35 (d, J = 5.8, 1H), 8.08 (d, J = 9.0 Hz, 1H), 7.77 (d, J = 2.0 Hz, 1H), 7.39 (dd, J = 2.0 Hz, J = 8.8 Hz, 1H), 6.51 (d, J = 5.5 Hz, 1H), 3.65 (t, J = 6.5, 2H), 3.39 (t, J = 7.0, 2H), 1.83 (m, 2H), 1.69 (m, 2H); ^{13}C NMR (100 MHz, CD_3SOCD_3): δ = 151.29, 151.04, 148.23, 134.86, 126.17, 124.54, 122.87, 117.33, 98.24, 61.23, 42.45, 29.63, 24.54; MS (LTQ): m/z calculated for $C_{13}H_{16}ClN_2O^+$ $[M+H]^+$ 251.09; found 251.02.

7.1.5. Synthesis of N-(2-bromoethyl)-7-chloroquinolin-4-amine [23] (3a)

Hydrobromic acid (0.88 mL, 16.2 mmol) and then sulphuric acid (0.29 mL, 5.5 mmol) was added dropwise to **2a** (0.67 g, 2.6 mmol), under cold conditions. The reaction was then heated for 4 h at 165 °C under reflux. The reaction medium was quenched by adding $NaHCO_3$ solution slowly and the pH was adjusted around 7. The reaction mixture was then extracted with dichloromethane dried over Na_2SO_4 and concentrated under vacuum to obtain the desired product **3a** in 85–95% yield as a white solid [19]. ^{1}H NMR (400 MHz, $CDCl_3$) δ = 8.59 (d, J = 5.3, 1H), 8.01 (d, J = 2.5 Hz, 1H), 7.74 (d, J = 9.0 Hz, 1H), 7.44 (m, 1H), 6.46 (d, J = 5.3 Hz, 1H), 3.80 (t, J = 5.8, 2H), 3.72 (t, J = 5.8, 2H); ^{13}C NMR (100 MHz, CD_3SOCD_3): δ = 152.27, 150.315, 149.21, 134.17, 127.74, 124.94, 117.75, 99.36, 44.48, 31.72; MS (LTQ): m/z calculated for $C_{11}H_{11}ClN_2O^+$ $[M+H]^+$ 285.57; found 285.14.

The remaining quinoline aminoalkylbromide derivatives (**3b-i**) were prepared following this typical procedure. Intermediates **3b-i** were determined by change in the TLC pattern and LTQ, thus were directly taken to the next step for synthesis of bromide derivatives.

7.1.6. Synthesis of N-(1-Amidino-2-thiourea-ethyl)-7-chloroquinol-4-amine (4a)

3a (200 mg, 1 mmol) was added to acetonitrile and 1-Amidino-2-thiourea (0.7 eq., 82 mg) and refluxed at 100 °C for 12–24 h. TLC was monitored at regular interval for the consumption of 1-Amidino-2-thiourea was consumed. The reaction mixture was then concentrated under vacuum to obtain a white solid. Successive washings by DCM, followed by acetonitrile and ethyl acetate resulted into the final product **4a** as a white solid in 55% yield [8a,20]. ^{1}H NMR (400 MHz, CD_3SOCD_3) δ = 8.37 (d, J = 5.5 Hz, 1H), 8.29 (d, J = 9.0 Hz, 1H), 7.79 (s, 1H), 7.64 (s, 1H), 7.43 (d, J = 10.5, 1H), 6.52 (d, J = 5.5, 1H), 3.60 (m, 2H), 3.07 (m, 2H); ^{13}C NMR (100 MHz, CD_3SOCD_3): δ = 164.09, 162.73, 155.84, 143.59, 139.05, 138.57, 127.50, 126.10, 119.69, 115.87, 99.49, 43.13, 28.98; IR (ATR) υ (cm^{-1}) 3206, 2912, 1607; MS (LTQ): m/z calculated for $C_{13}H_{16}N_6SCl^+$ $[M+H]^+$ 323.07; found 323.08; MS ES+ (HRMS): m/z calculated for $C_{13}H_{16}N_6SCl^+$ $[M+H]^+$ 323.0846; found 323.0837.

The remaining quinoline aminoalkylguanylthiourea derivatives (**4b-i**) were prepared following procedure as mentioned above.

7.1.7. N-(1-Amidino-2-thiourea-propyl)-7-chloroquinol-4-amine (4b)

White solid; 65% yield; ^{1}H NMR (400 MHz, CD_3OD) δ = 8.42 (m, 2H), 7.88 (s, 1H), 7.63 (d, J = 10.3 Hz, 1H), 6.86 (d, J = 6.8, 1H), 3.63 (t, J = 6.5, 2H), 3.10 (t, J = 7.3, 2H), 2.18 (m, 2H); ^{13}C NMR (100 MHz, MeOD): δ = 164.21, 162.62, 155.75, 143.52, 139.02, 138.42, 127.27, 126.25, 119.51, 115.94, 99.17, 49.04, 42.34, 28.36; IR (ATR) υ (cm^{-1}) 3108, 2937, 2194, 1610, 1585, 1553, 1449; MS (LTQ): m/z calculated for $C_{14}H_{18}N_6SCl^+$ $[M+H]^+$ 337.09; found 337.04; MS ES+ (HRMS): m/z calculated for $C_{14}H_{18}N_6SCl^+$ $[M+H]^+$ 337.1002; found 337.0996.

7.1.8. N-(1-Amidino-2-thiourea-butyl)-7-chloroquinol-4-amine (4c)

Oily liquid; 52% yield; ^{1}H NMR (400 MHz, CD_3OD) δ = 8.31 (d, J = 9.3, 1H), 8.25 (d, J = 6.2 Hz, 1H), 7.74 (d, J = 2.2 Hz, 1H), 7.36 (dd, J = 2.3, J = 9.3, 1H), 6.54 (d, J = 6.0, 1H), 3.76 (t, J = 4.0, 4H), 2.09 (m, 4H); ^{13}C NMR (100 MHz, MeOD): δ = 153.47, 147.06, 135.65, 127.71, 125.03, 123.79, 123.27, 118.22, 102.34, 98.25, 61.28, 52.43, 34.38, 25.42; IR (ATR) υ (cm^{-1}) 3318, 2944, 2834, 2195, 1614, 1587, 1562, 1451; MS (LTQ): m/z calculated for $C_{15}H_{20}N_6SCl^+$ $[M+H]^+$ 351.11; found 351.14; MS ES+ (HRMS): m/z calculated for $C_{15}H_{20}N_6SCl^+$ $[M - C_2H_6N_4S]^+$ 233.0846; found 233.0832. (HRMS spectra is showing the peak of the fragment after losing $C_2H_6N_4S$ unit.)

7.1.9. N-(1-Amidino-2-thiourea-ethyl)-7-trifluoromethylquinol-4-amine (4d)

White solid; 60% yield; ^{1}H NMR (400 MHz, CD_3OD) δ = 8.68 (d, J = 8.8, 1H), 8.57 (d, J = 7.3, 1H), 8.24 (s, 1H), 7.96 (d, J = 8.8, 1H), 7.10 (d, J = 7.0, 1H), 3.99 (t, J = 7.5, 2H), 3.39 (t, J = 7.6, 2H);^{13}C NMR (100 MHz, MeOD): δ = 166.84, 164.51, 156.05, 154.79, 154.73, 145.73, 143.66, 138.02, 134.28, 123.51, 119.09, 117.87, 99.65, 42.98, 28.36; IR (ATR) υ (cm^{-1}) 3283, 3159, 2921, 2794, 1613, 1507, 1446; MS (LTQ): m/z calculated for $C_{14}H_{16}N_6SF_3^+$ $[M+H]^+$ 357.11; found 357.08; MS ES+ (HRMS): m/z calculated for $C_{14}H_{16}N_6SF_3^+$ $[M+H]^+$ 357.1109; found 357.1105.

7.1.10. N-(1-Amidino-2-thiourea-propyl)-7-trifluoromethylquinol-4-amine (4e)

White solid; 65% yield; ^{1}H NMR (400 MHz, CD_3SOCD_3) δ = 8.64 (d, J = 9.0, 1H), 8.50 (d, J = 6.8, 1H), 8.19 (s, 1H), 7.88 (d, J = 8.8, 1H),

6.93 (d, J = 6.8, 1H), 4.03 (t, J = 6.3, 2H), 3.09 (t, J = 7.0, 2H), 2.18 (m, 2H), ^{13}C NMR (100 MHz, CD_3SOCD_3): δ = 164.09, 162.67, 155.80, 144.09, 137.74, 126.30, 112.39, 119.49, 118.03, 99.96, 42.52, 28.36, 28.89; IR (ATR) υ (cm^{-1}) 3296, 3176, 2252, 1644; MS (LTQ): m/z calculated for $C_{14}H_{17}N_6SCF_3^+$ $[M+H]^+$ 371.13; found 371.03; MS ES + (HRMS): m/z calculated for $C_{15}H_{18}N_6SF_3^+$ $[M+H]^+$ 371.1266; found 371.1261.

7.1.11. N-(1-Amidino-2-thiourea-butyl)-7-trifluoromethylquinol-4-amine (4f)

Oily Liquid; 58% yield; ^{1}H NMR (400 MHz, CD_3OD) δ = 8.69 (d, J = 8.5, 1H), 8.53 (d, J = 6.3 Hz, 1H), 8.21 (s, 1H), 7.93 (d, J = 8.5, 1H), 7.00 (d, J = 6.3, 1H), 3.69 (t, J = 6.3, 2H), 3.11 (t, J = 7.0, 2H), 1.93 (m, 4H);^{13}C NMR (100 MHz, MeOD): δ = 162.86, 162.03, 152.20, 144.41, 140.04, 128.01, 125.62, 124.19, 122.67, 119.60, 93.83, 42.12, 30.41, 29.23, 26.76; IR (ATR) υ (cm^{-1}) 3115, 2938, 2193, 2150, 1612, 1568, 1454; MS (LTQ): m/z calculated for $C_{16}H_{20}N_6SF_3^+$ $[M+H]^+$385.14; found 385.09; MS ES+ (HRMS): m/z calculated for $C_{16}H_{20}N_6SF_3^+$ $[M+H]^+$385.1422; found 385.1409.

7.1.12. N-(1-Amidino-2-thiourea-ethyl)-(2,8-Bis-(trifluoromethyl))quinol-4-amine (4g)

Brown solid; 20% yield; ^{1}H NMR (400 MHz, CD_3OD) δ = 8.39 (d, J = 8.0, 1H), 8.09 (d, J = 7.3, 1H), 7.63 (t, J = 8.0, 1H), 7.13 (s, 1H), 3.80 (t, J = 7.8, 2H), 3.28 (t, J = 7.8, 2H);^{13}C NMR (100 MHz, CD_3SOCD_3): δ = 165.42, 163.63, 151.97, 144.39, 128.32, 125.43, 124.33, 119.51, 94.38, 42.29, 28.30; IR (ATR) υ (cm^{-1}) 3266, 3105, 2195, 1687, 1592, 1544, 1526, 1504; MS (LTQ): m/z calculated for $C_{15}H_{15}N_6SF_6^+$ $[M+H]^+$ 425.09; found 424.99.

7.1.13. N-(1-Amidino-2-thiourea-propyl)-(2,8-Bis-(trifluoromethyl)) quinol-4-amine (4h)

White solid; 50% yield; ^{1}H NMR (400 MHz, CD_3OD) δ = 8.45 (d, J = 8.5, 1H) 8.10 (d, J = 7.3, 1H), 7.63 (t, J = 7.6, 1H), 6.87 (s, 1H), 3.57 (t, J = 7.0, 2H), 3.17 (t, J = 6.8, 2H), 2.18 (m, 2H); ^{13}C NMR (100 MHz, MeOD): δ = 166.19, 162.89, 152.16, 148.96, 148.62, 144.39, 128.28, 125.54, 124.24, 119.62, 93.92, 41.26, 28.18, 27.87; IR (ATR) υ (cm^{-1}) 3400, 2951, 2843, 2077, 1645, 1454, 1412; MS (LTQ): m/z calculated for $C_{16}H_{17}N_6SF_6^+$ $[M+H]^+$439.11; found 439.07; MS ES+ (HRMS): m/z calculated for $C_{16}H_{17}N_6SF_6^+$ $[M+H]^+$439.1140; found 439.1141.

7.1.14. N-(1-Amidino-2-thiourea-propyl)-(2,8-Bis-(trifluoromethyl)) quinol-4-amine (4i)

Yellow Oily Liquid; 50% yield; ^{1}H NMR (400 MHz, CD_3OD) δ = 8.46 (d, J = 8.6, 1H) 8.09 (d, J = 7.3, 1H), 7.62 (t, J = 8.0, 1H), 6.87 (s, 1H), 3.47 (t, J = 6.2, 2H), 3.10 (t, J = 7.0, 2H), 1.88 (m, 4H); ^{13}C NMR (100 MHz, MeOD): δ = 166.41, 162.87, 152.28, 144.40, 128.26, 128.10, 125.61, 125.39, 124.18, 122.67, 119.59, 93.84, 93.03, 42.12, 30.42, 26.95, 21.22; IR (ATR) υ (cm^{-1}) 3303, 3162, 2300, 2194, 1621, 1594, 1542; MS (LTQ): m/z calculated for $C_{17}H_{19}N_6SF_6^+$ $[M+H]^+$ 453.42; found 453.09; MS ES+ (HRMS): m/z calculated for $C_{17}H_{19}N_6SF_6^+$ $[M+H]^+$ 453.1296; found 453.1295.

8. Computational methodology

8.1. Molecular docking

Molecular docking was performed using Schrödinger software package (GLIDE module) [14]. Initial 3D structures of all the molecules were obtained by (energy minimization) geometry optimization using OPLS_2005 force field. LigPrep module of maestro is used to prepare (standard-data file (.sdf) format) the 3D structures of the molecules implementing OPLS_2005 force field and keeping ionic states of the ligands at pH values 7.0 ± 2.0. Conformational search of all the ligands was performed using confgen module of maestro and top five poses were chosen for docking in 1J3I and 1J3K. Two different crystal structures of *Pf*DHFR were chosen i.e. 1J3I for wild type and 1J3K for quadruple mutant *Pf*DHFR, both with WR99210 as the co-crystallized ligand. Missing residues were added using prime module of maestro and incorporating FASTA peptide sequence for both 1J3I and 1J3K. The protein structural preparation was carried out using the protein preparation wizard in maestro during which only chain A (PDB ID 1J3I and 1J3K) was considered for the docking purpose. Generate states option was used to obtain the docked structure of the reference ligand in the crystalized protein at pH 7.0 ± 2.0. All the water molecules were removed, hydrogen atoms were added and the final protein complex with WR99210 and NADPH was optimized and minimized (10,000 cycles). The grid was generated taking the reference ligand as core, with the grid size of 10 Å. Glide module (Grid-based Ligand Docking with Energetics), was used to perform molecular docking with standard precision mode. The docking protocol was validated by re-docking the bound ligand (WR99210) and comparing the RMSD value with the X-ray crystallographic conformation of the ligand. The best suited pose and corresponding G_{score} values are considered as standard for comparison with the docking scores of **4a-i**.

9. Molecular dynamics (MD) simulations

MD simulations were carried out using AMBER 11.0 program [24]. Ligand preparation was done using "leaprc.gaff" (generalized amber force field) force field and enzyme preparation was done using "leaprc.ff03" [25]. A 10 Å cubic box of TIP3P water was positioned to surround each system and chloride ions were added to neutralize the system. Minimization (500 steps of steepest descent followed by 500 steps of conjugate gradient method), 50 ps of heating, and 50 ps of density run with weak restraints on the complex followed by 4 ns constant pressure equilibration at 300 K were performed on each complex. A cut-off of 8.0 Å was used for MD simulations. Particle mesh Ewald method was exploited to include all long-range electrostatics. The system was maintained at 300 K temperature using Langevin thermostat. All the conditions applied in the final phase of equilibration were used for production run, and the coordinates were recorded every 10 ps. The periodic boundary conditions were used during MD simulations. Root mean squared deviation plots (RMSD) were constructed before submitting for the production run of 24 ns to make sure that system has equilibrated.

MM-PBSA calculations: The $\Delta G_{Bind\text{-}PB}$ between ligand and receptor to form a complex can be calculated as follows:

$$\Delta G_{Bind} = \Delta E_{MM} + \Delta G_{SOL(PB)} - T\Delta S$$

$$\Delta E_{MM} = \Delta E_{internal} + \Delta E_{electrostatic} + \Delta E_{vdw}$$

$$\Delta G_{SOL(PB)} = \Delta G_{PB} + \Delta G_{SA(PB)}$$

where ΔE_{MM} is the total gas-phase energy, $\Delta G_{SOL(PB)}$ is the sum of non-polar and polar contributions to solvation calculated by PB. $\Delta E_{internal}$ is the internal energy arising from bond angle and dihedral terms in the MM force field and is zero in case of single trajectory approach. $\Delta E_{electrostatic}$ is electrostatic energy as calculated by the molecular mechanics force field. ΔE_{vdw} is van der Waals contribution from MM. ΔG_{PB} is the non-polar contribution to the solvent free energy and was estimated by SASA determined using a water probe radius of 1.4 Å. The surface tension constant γ was set to be 0.00542 kcal/mol/Å^2. $\Delta G_{SOL(PB)}$ is the electrostatic contribution to the solvation energy calculated by the PB method. Dielectric constants for solute and solvent were set to be 1 and 80, respectively. Vibrational entropy contributions can be estimated by classical statistical thermodynamics, using normal mode analysis. As the main goal is to analyse the comprehensive interaction features, the entropy contribution was not included in the study due to high computational cost.

10. Biological evaluation- determination of *in vitro* antimalarial activity and cytotoxicity

The compounds were tested for *in vitro* antimalarial activity against the D6 (chloroquine-sensitive) and W2 (chloroquine-resistant) strains of *P. falciparum*. The 96-well microplate assay is based on evaluation of the effect of the compound on growth of asynchronous cultures of *P. falciparum* determined by the assay of parasite lactate dehydrogenase (pLDH) activity [5c]. The stock solutions of the test were prepared in DMSO, appropriate dilutions were prepared in serum-free RPMI-1640 medium and the compounds were added to the cultures of *P. falciparum* (2% haematocrit, 2% 84 parasitaemia) set up in clear, flat-bottomed, 96-well plates. The plates were placed into the humidified chamber and flushed with a gas mixture of 90% N_2, 5% CO_2 and 5% O_2. The cultures were incubated at 37 °C for 48 h. Growth of the parasite in each well was determined by pLDH assay using Malstat® reagent as described earlier [9a]. The medium and red blood cell (RBC) controls were also set up in each plate. The standard anti-malarial agents, CQ and pyrimethamine, were tested as the positive controls, while DMSO was tested as the negative control. The antimalarial efficacy (expressed as IC_{50} value) was determined by the dose response analysis with XLfit©. The compounds were simultaneously tested for cytotoxicity against vero cells [9b].

Acknowledgements

The University Grants Commission is gratefully acknowledged for the financial support to Shweta Bhagat (UGC, Grant No. 43395). The authors thank department of science and technology, government of India, New Delhi, India for financial support and NIPER, S. A. S. Nagar for infrastructural facilities. Technical assistance of John Trott and facilities provided by the National Center for Natural Products Research for the antimalarial and cytotoxicity assays are gratefully acknowledged.

Appendix A. Supplementary material

Supplementary data to this article can be found online at https://doi.org/10.1016/j.bioorg.2019.103094.

References

[1] World malaria report 2018, World Health Organization, Geneva, 2018, p. 166.
[2] Malaria vaccine: WHO position paper, Wkly. Epidemiol. Rec. 91(4) (2016) pp. 33–52.
[3] (a) T.E. Wellems, C.V. Plowe, Chloroquine-resistant Malaria, J. Infect. Dis. 184 (6) (2001) 770–776;
(b) V. Narasimhan, A. Attaran, Roll back malaria? The scarcity of international aid for malaria control, Malar. J. 2 (1) (2003) 8;
(c) M. Chinappi, A. Via, P. Marcatili, et al., On the mechanism of chloroquine resistance in plasmodium falciparum, PLoS ONE 5 (11) (2010) e14064;
(d) F. Nuwaha, The challenge of chloroquine-resistant malaria in sub-Saharan Africa, Health Policy Plan. 16 (1) (2001) 1–12;
(e) H.M. Staines, S. Krishna, Treatment and Prevention of Malaria, 1st ed., Springer Basel, Basel, 2012.
[4] (a) F.J. Gamo, L.M. Sanz, J. Vidal, et al., Thousands of chemical starting points for antimalarial lead identification, Nature 465 (7296) (2010) 305–310;
(b) T.N. Wells, R. Hooft van Huijsduijnen, W.C. Van Voorhis, Malaria medicines: a glass half full? Nat. Rev. Drug Discov. 14 (6) (2015) 424–442;
(c) S. Yeung, W. Pongtavornpinyo, I.M. Hastings, et al., Antimalarial drug resistance, artemisinin-based combination therapy, and the contribution of modeling to elucidating policy choices, Am. J. Trop. Med. Hyg. 71 (2 Suppl) (2004) 179–186.
[5] (a) E. Talundzic, S.A. Okoth, K. Congpuong, et al., Selection and spread of Artemisinin-resistant alleles in Thailand prior to the global artemisinin resistance containment campaign, PLoS Pathog. 11 (4) (2015) e1004789;
(b) D. Agarwal, M. Sharma, S.K. Dixit, et al., In vitro synergistic effect of fluoroquinolone analogues in combination with artemisinin against Plasmodium falciparum; their antiplasmodial action in rodent malaria model, Malar. J. 14 (1) (2015) 48;
(c) R. Sahu, L.A. Walker, B.L. Tekwani, In vitro and in vivo anti-malarial activity of tigecycline, a glycylcycline antibiotic, in combination with chloroquine, Malar. J. 13 (1) (2014) 414;
(d) O. Miotto, J. Almagro-Garcia, M. Manske, et al., Multiple populations of artemisinin-resistant Plasmodium falciparum in Cambodia, Nat. Genet. 45 (2013) 648–655;
(e) C. Teixeira, N. Vale, B. Pérez, et al., "Recycling" Classical Drugs for Malaria, Chem. Rev. 114 (22) (2014) 11164–11220;
(f) N.J. White, Artemisinin resistance–the clock is ticking, Lancet 376 (9758) (2010) 2051–2052.
[6] (a) K.V. Sashidhara, M. Kumar, R.K. Modukuri, et al., Antiplasmodial activity of novel keto-enamine chalcone-chloroquine based hybrid pharmacophores, Bioorg. Med. Chem. 20 (9) (2012) 2971–2981;
(b) F. Bellot, F. Cosledan, L. Vendier, et al., Trioxaferroquines as new hybrid antimalarial drugs, J. Med. Chem. 53 (10) (2010) 4103–4109;
(c) J. Chadwick, R.K. Amewu, F. Marti, et al., Antimalarial mannoxanes: hybrid antimalarial drugs with outstanding oral activity profiles and a potential dual mechanism of action, ChemMedChem 6 (8) (2011) 1357–1361;
(d) S. Vandekerckhove, M. D'Hooghe, Quinoline-based antimalarial hybrid compounds, Bioorg. Med. Chem. 23 (16) (2015) 5098–5119;
(e) V.V. Kouznetsov, A. Gomez-Barrio, Recent developments in the design and synthesis of hybrid molecules based on aminoquinoline ring and their antiplasmodial evaluation, Eur. J. Med. Chem. 44 (8) (2009) 3091–3113;
(f) B.C. Perez, C. Teixeira, I.S. Albuquerque, et al., N-cinnamoylated chloroquine analogues as dual-stage antimalarial leads, J. Med. Chem. 56 (2) (2013) 556–567;
(g) D.H. Peyton, Reversed chloroquine molecules as a strategy to overcome resistance in malaria, Curr. Top. Med. Chem. 12 (5) (2012) 400–407;
(h) P.F. Salas, C. Herrmann, J.F. Cawthray, et al., Structural characteristics of chloroquine-bridged ferrocenophane analogues of ferroquine may obviate malaria drug-resistance mechanisms, J. Med. Chem. 56 (4) (2013) 1596–1613.
[7] D. Payne, Spread of chloroquine resistance in *Plasmodium falciparum*, Parasitol. Today 3 (8) (1987) 241–246.
[8] (a) L. Adane, S. Bhagat, M. Arfeen, et al., Design and synthesis of guanylthiourea derivatives as potential inhibitors of Plasmodium falciparum dihydrofolate reductase enzyme, Bioorg. Med. Chem. Lett. 24 (2) (2014) 613–617;
(b) M. Arfeen, D.S. Patel, S. Abbat, et al., Importance of cytochromes in cyclization reactions: Quantum chemical study on a model reaction of proguanil to cycloguanil, J. Comput. Chem. 35 (28) (2014) 2047–2055;
(c) S. Bhagat, M. Arfeen, L. Adane, et al., Guanylthiourea derivatives as potential antimalarial agents: Synthesis, in vivo and molecular modelling studies, Eur. J. Med. Chem. 135 (2017) 339–348;
(d) T. Dasgupta, P. Chitnumsub, S. Kamchonwongpaisan, et al., Exploiting structural analysis, in silico screening, and serendipity to identify novel inhibitors of drug-resistant falciparum malaria, ACS Chem. Biol. 4 (1) (2009) 29–40.
[9] (a) M.T. Makler, D.J. Hinrichs, Measurement of the lactate dehydrogenase activity of plasmodium falciparum as an assessment of parasitemia, Am. J. Trop. Med. Hyg. 48 (2) (1993) 205–210;
(b) V. Patil, W. Guerrant, P.C. Chen, et al., Antimalarial and antileishmanial activities of histone deacetylase inhibitors with triazole-linked cap group, Bioorg. Med. Chem. 18 (1) (2010) 415–425.
[10] (a) S. Abbat, C.K. Jaladanki, P.V. Bharatam, Exploring PfDHFR reaction surface: A combined molecular dynamics and QM/MM analysis, J. Mol. Graph. Model. 87 (2019) 76–88;
(b) W. Mokmak, S. Chunsrivirot, S. Hannongbua, et al., Molecular Dynamics of Interactions between Rigid and Flexible Antifolates and Dihydrofolate Reductase from Pyrimethamine-Sensitive and Pyrimethamine-Resistant Plasmodium falciparum, Chem. Biol. Drug Des. 84 (4) (2014) 450–461;
(c) D.S. Peterson, W.K. Milhous, T.E. Wellems, Molecular basis of differential resistance to cycloguanil and pyrimethamine in Plasmodium falciparum malaria, Proc. Natl. Acad. Sci. USA 87 (8) (1990) 3018–3022;
(d) G. Rastelli, W. Sirawaraporn, P. Sompornpisut, et al., Interaction of pyrimethamine, cycloguanil, WR99210 and their analogues with Plasmodium falciparum dihydrofolate reductase: structural basis of antifolate resistance, Bioorg. Med. Chem. 8 (5) (2000) 1117–1128;
(e) S. Abbat, S. Bhagat, P.V. Bharatam, PfDHFR enzyme inhibitors: rational design using pharmacoinformatic tools, in: Atta-ur-Rahman, R. A.B., C. M.I., et al. (Eds.), Frontiers in Medicinal Chemistry, Bentham Science, 2015, pp. 228–273.
[11] (a) S. Abbat, V. Jain, P.V. Bharatam, Origins of the specificity of inhibitor P218 toward wild-type and mutant PfDHFR: a molecular dynamics analysis, J. Biomol. Struct. Dyn. 33 (9) (2015) 1913–1928;
(b) L. Adane, P.V. Bharatam, Tautomeric preferences and electron delocalization in biurets, thiobiurets, and dithiobiurets: An ab initio study, Int. J. Quantum Chem. 108 (7) (2008) 1277–1286;
(c) M. Arfeen, D.S. Patel, S. Abbat, et al., Importance of cytochromes in cyclization reactions: quantum chemical study on a model reaction of proguanil to cycloguanil, J. Comput. Chem. 35 (28) (2014) 2047–2055;
(d) P.V. Bharatam, D.S. Patel, P. Iqbal, Pharmacophoric features of biguanide derivatives: an electronic and structural analysis, J. Med. Chem. 48 (24) (2005) 7615–7622;
(e) S. Bhatia, P.V. Bharatam, Possibility of the existence of donor-acceptor interactions in bis(azole)amines: an electronic structure analysis, J. Org. Chem. 79 (11) (2014) 4852–4862;
(f) A. Mehdi, L. Adane, D.S. Patel, et al., Electronic structure and reactivity of guanylthiourea: A quantum chemical study, J. Comp. Chem. 31 (6) (2010) 1259–1267;
(g) D.S. Patel, P.V. Bharatam, Divalent N(I) compounds with two lone pairs on nitrogen, J. Phys. Chem. A 115 (26) (2011) 7645–7655;
(h) M. Arfeen, R. Patel, T. Khan, P.V. Bharatam, Molecular dynamics simulation studies of GSK-3β ATP competitive inhibitors: understanding the factors contributing to selectivity, J. Biomol. Struct. Dyn. 33 (12) (2015) 2578–2593.

[12] (a) L. Adane, P.V. Bharatam, Modelling and informatics in the analysis of P. falciparum DHFR Enzyme Inhibitors, Curr. Med. Chem. 15 (16) (2008) 1552–1569;
(b) L. Adane, P.V. Bharatam, 3D-QSAR analysis of cycloguanil derivatives as inhibitors of A16V + S108T mutant Plasmodium falciparum dihydrofolate reductase enzyme, J. Mol. Graph. Model. 28 (4) (2009) 357–367;
(c) L. Adane, P.V. Bharatam, Computer-aided molecular design of 1H-imidazole-2,4-diamine derivatives as potential inhibitors of Plasmodium falciparum DHFR enzyme, J. Mol. Model. 17 (4) (2011) 657–667;
(d) L. Adane, P.V. Bharatam, V. Sharma, A common feature-based 3D-pharmacophore model generation and virtual screening: identification of potential PfDHFR inhibitors, J. Enzyme Inhib. Med. Chem. 25 (5) (2010) 635–645;
(e) L. Adane, D.S. Patel, P.V. Bharatam, Shape-and chemical feature-based 3D-pharmacophore model generation and virtual screening: identification of potential leads for P. falciparum DHFR Enzyme Inhibition, Chem. Biol. Drug Des. 75 (1) (2010) 115–126;
(f) G. Rastelli, S. Pacchioni, W. Sirawaraporn, et al., Docking and database screening reveal new classes of plasmodium falciparum dihydrofolate reductase inhibitors, J. Med. Chem. 46 (14) (2003) 2834–2845;
(g) Y. Yuthavong, B. Tarnchompoo, T. Vilaivan, et al., Malarial dihydrofolate reductase as a paradigm for drug development against a resistance-compromised target, Proc. Natl. Acad. Sci. USA 109 (42) (2012) 16823–16828;
(h) J. Yuvaniyama, P. Chitnumsub, S. Kamchonwongpaisan, et al., Insights into antifolate resistance from malarial DHFR-TS structures, Nat. Struct. Biol. 10 (5) (2003) 357–365.
[13] M.J. Frisch, G.W. Trucks, H.B. Schlegel, et al., Gaussian 09, Gaussian Inc, Wallingford, CT, USA, 2009.
[14] (a) S. Manohar, S.I. Khan, D.S. Rawat, Synthesis of 4-aminoquinoline-1,2,3-triazole and 4-aminoquinoline-1,2,3-triazole-1,3,5-triazine hybrids as potential antimalarial agents, Chem. Biol. Drug Des. 78 (1) (2011) 124–136;
(b) S. Manohar, U.C. Rajesh, S.I. Khan, et al., Novel 4-aminoquinoline-pyrimidine based hybrids with improved in vitro and in vivo antimalarial activity, ACS Med. Chem. Lett. 3 (7) (2012) 555–559;
(c) S.I. Pretorius, W.J. Breytenbach, C. de Kock, et al., Synthesis, characterization and antimalarial activity of quinoline–pyrimidine hybrids, Bioorg. Med. Chem. 21 (1) (2013) 269–277;
(d) M. Sharma, K. Chauhan, S.S. Chauhan, et al., Synthesis of hybrid 4-anilinoquinoline triazines as potent antimalarial agents, their in silico modeling and bioevaluation as Plasmodium falciparumtransketolase and β-hematin inhibitors, MedChemComm 3 (1) (2012) 71–79;
(e) K. Singh, H. Kaur, K. Chibale, et al., Synthesis of 4-aminoquinoline-pyrimidine hybrids as potent antimalarials and their mode of action studies, Eur. J. Med. Chem. 66 (2013) 314–323;
(f) R. Thelingwani, B. Bonn, K. Chibale, et al., Physicochemical and drug metabolism characterization of a series of 4-aminoquinoline-3-hydroxypyridin-4-one hybrid molecules with antimalarial activity, Expert Opin. Drug Metab. Toxicol. 10 (10) (2014) 1313–1324.
[15] (a) R.A. Friesner, J.L. Banks, R.B. Murphy, et al., Glide: a new approach for rapid, accurate docking and scoring. 1. Method and assessment of docking accuracy, J. Med. Chem. 47 (7) (2004) 1739–1749;
(b) T.A. Halgren, R.B. Murphy, R.A. Friesner, et al., Glide: a new approach for rapid, accurate docking and scoring. 2. Enrichment factors in database screening, J. Med. Chem. 47 (7) (2004) 1750–1759.
[16] P.V. Bharatam, S. Khanna, S.M. Francis, Modeling and informatics in drug design, in: S.C. Gad (Ed.), Preclinical Development Handbook, John Wiley & Sons Inc, Hoboken, New Jersey, 2007, pp. 1–45.
[17] J. Mao, Y. Wang, B. Wan, et al., Design, synthesis, and pharmacological evaluation of mefloquine-based ligands as novel antituberculosis agents, ChemMedChem 2 (11) (2007) 1624–1630.
[18] E.M. Guantai, K. Ncokazi, T.J. Egan, et al., Enone- and chalcone-chloroquinoline hybrid analogues: in silico guided design, synthesis, antiplasmodial activity, in vitro metabolism, and mechanistic studies, J. Med. Chem. 54 (10) (2011) 3637–3649.
[19] J. Cazelles, F. Cosledan, B. Meunier, et al., Dual molecules containing peroxy derivative, the synthesis and therapeutic applications thereof, US Patent 0021423 A1, 2007.
[20] (a) R.L. Summerfield, D.M. Daigle, S. Mayer, et al., A 2.13 Å structure of E. coli dihydrofolate reductase bound to a novel competitive inhibitor reveals a new binding surface involving the M20 loop region, J. Med. Chem. 49 (24) (2006) 6977–6986;
(b) L.D.S. Yadav, V.K. Rai, Thiourea to bicyclic scaffolds: highly regio- and stereoselective routes to dithiazolopyrimidines, Tetrahedron 63 (29) (2007) 6924–6931.
[21] S. Eswaran, A.V. Adhikari, I.H. Chowdhury, et al., New quinoline derivatives: synthesis and investigation of antibacterial and antituberculosis properties, Eur. J. Med. Chem. 45 (8) (2010) 3374–3383.
[22] D.H. Peyton, S. Burgess, Quinoline Derivatives and Uses Thereof, State of Oregon acting by and through the State Board of Higher Education on behalf of, Portland State University, Portland, OR (US) USA, 2011.
[23] J. Cazelles, F. Cosledan, B. Meunier, et al., Dual molecules containing peroxy derivative, the synthesis and therapeutic applications thereof, Sanofi-Aventis, Paris (FR), 2011.
[24] D.A. Case, T.A. Darden, T.E. Cheatham, et al., AMBER 2011, University of California, San Francisco, 2010.
[25] D.A. Case, T.E. Cheatham, T. Darden, et al., The Amber biomolecular simulation programs, J. Comput. Chem. 26 (2005) 1668–1688.